Layer-dependent electronic structure of an atomically heavy two-dimensional dichalcogenide

Po-Chun Yeh, Wencan Jin, Nader Zaki, Datong Zhang, Jonathan T. Liou, Jerzy T. Sadowski, Abdullah Al-Mahboob, Jerry I. Dadap, Irving P. Herman, Peter Sutter, and Richard M. Osgood, Jr.

Phys. Rev. B **91**, 041407 — Published 20 January 2015

DOI: 10.1103/PhysRevB.91.041407

Layer-dependent electronic structure of an atomically heavy 2D dichalcogenide

Po-Chun Yeh,[1] Wencan Jin,[2] Nader Zaki,[2] Datong Zhang,[2] Jonathan. T. Liou[1], Jerzy T. Sadowski,[3] Abdullah Al-Mahboob,[3] Jerry I. Dadap,[2] Irving P. Herman,[2] Peter Sutter,[3] and Richard M. Osgood, Jr.[1,2,*]

[1] Department of Electrical Engineering, Columbia University, New York, New York 10027, USA

[2] Department of Applied Physics and Applied Mathematics, Columbia University, New York, New York 10027, USA

[3]Center for Functional Nanomaterials, Brookhaven National Laboratory, Upton, New York 11973, USA

Keywords: WSe_2, ARPES, SPE-LEEM, layer dependence, transfer process, LEEM, LEED

Abstract

We report angle-resolved photoemission spectroscopic measurements of the evolution of the thickness-dependent electronic band structure of the heavy-atom two-dimensional layered, dichalcogenide, tungsten-diselenide (WSe_2). Our data, taken on mechanically exfoliated WSe_2 single-crystals, provide direct evidence for shifting of the valence-band maximum from $\bar{\Gamma}$ (multilayer WSe_2), to $\bar{K}$, (single-layer WSe_2). Further, our measurements also set a lower bound on the energy of the direct band-gap and provide direct measurement of the hole effective mass.

Single layers of two-dimensional metal dichalcogenides (TMDCs) such as MoS_2, have emerged as a new class of non-centrosymmetric direct-bandgap materials with potential photonic and spintronic applications.[1][2] Among the TMDC family, tungsten-based dichalcogenides, such as WSe_2, exhibit high in-plane carrier mobility and allow electrostatic modulation of the conductance,[3][4] characteristics, which make them promising for device applications. For example, bulk WSe_2 possesses an indirect bandgap of 1.2 eV [1][5] and has been used as the channel of a field-effect transistor (FET) with an intrinsic hole mobility of up to 500 $cm^2/(V\text{-}s)$.[6] By comparison, WSe_2, in its monolayer form (ML), should have a direct band gap, as predicted by theory,[7][8][9][10][11][12] and a promising intrinsic hole mobility of 250 $cm^2/(V\text{-}s)$, as recently demonstrated in the performance of top-gated FETs[4]. In addition, ML WSe_2 has been demonstrated to be the first TMDC material possessing ambipolar, i.e., both p-type and n-type conducting behavior,[4][12] thus making it possible to design additional electronic functionality, such as p-n junctions or complementary logic circuits.

Despite these intriguing characteristics, measurements of ML WSe_2 have generally been limited to probing of optical and transport properties.[4][5][6] In this paper, we report thickness-dependent measurements of the surface and electronic structure of exfoliated WSe_2, using low-energy electron microscopy (LEEM), diffraction (LEED), and micrometer-scale angle-resolved photoemission spectroscopy (μ-ARPES) of samples supported on a native-oxide terminated silicon substrate. Our experimental results provide direct evidence for a predicted valence-band maximum (VBM) symmetry-point change, which leads to an indirect-to-direct bandgap transition. Because TMDCs have a large carrier effective mass and reduced screening in two dimensions, electron–hole interactions are much stronger than in conventional semiconductors.[13][14][15] Our results allow us to obtain a direct measurement of the hole effective mass. Finally, our measurements allow us to directly infer a lower bound on the energy of the direct band gap.

Our measurements were performed using the spectroscopic photoemission and low-energy electron microscope (SPE-LEEM) system at the National Synchrotron Light Source (NSLS) beamline U5UA.[16][17] The spectrometer energy resolution of this instrument was set to 100 meV at 33 eV incident photon energy with a beam spot size of 1 μm in diameter. The momentum resolution is ~0.02 $Å^{-1}$. Exfoliated WSe_2 samples were transferred to a native-oxide covered Si substrate; prior to measurements, these samples were annealed at 350°C for ~12 hours under UHV conditions. The layer number of the sample is determined by Raman and photoluminescence spectroscopy.[18][19] Additional experimental details can be found in the Supplemental Materials section.

Sample quality and crystal orientation were examined using both LEEM and μ-LEED (Fig. 1). Diffraction patterns (at a primary electron energy of 48eV) of exfoliated WSe_2 flakes of 1-3ML and bulk are shown in Fig. 2a-d, respectively, and clearly display the six-fold crystal symmetry. At an electron energy of 48eV, the mean free path of the low-energy electrons is ~5.2Å,[20] which is comparable to the thickness of a single covalently bound Se-W-Se unit of monolayer WSe_2 (~7Å).[4][21] With increasing WSe_2 thickness, the LEED spots become sharper due, in part, to decreased scattering from the substrate.[22] This assertion is supported by the monotonically decreasing full-width-at-half- maximum (FWHM) of the (00) diffraction spot, plotted for different electron energies in Fig. 2e.[22]

The electronic structure of the top-lying valence bands of WSe_2 is derived from the W 5d and Se 4p orbitals[23][24], each of which possesses a strongly varying photon-energy-dependent photoionization cross-section,[25] as displayed in Fig. 3b. Prior work[25] has shown that the cross-section of the W 5d subshell is an order of magnitude larger than that of Se 4p at the photon energy of 33eV used in our experiments (indicated by the vertical line in Fig. 3b.) Thus the primary contributions to our μ-ARPES measurements, shown in Fig. 4, are from the W 5d orbitals. Angle-integrated photoemission spectra of 1ML WSe_2 along high symmetry directions and over the full Brillouin Zone (BZ) are shown in Fig. 3c. These spectra show a clear energy cut-off at about 1.8±0.1eV above the VBM, which we identify as the position of the Fermi level E_F. The bandgap of ML WSe_2 has previously been reported to be in the range of 1.4 to 2.3eV.[19][26][27] Based on our identification of the Fermi energy, the minimum bandgap value of WSe_2 must be greater than at least 1.8eV; this result also suggests that our exfoliated ML WSe_2 is heavily electron-doped, i.e. the Fermi level falls near the conduction band minimum.[28][29] The energy differences between the Fermi level (E_F) and the VBM for 2ML, 3ML, and bulk, are approximately 1.5eV, 1.5eV, and 1.1eV, respectively. Taking into account the previously reported bandgap energies of these materials, we find that these energy differences are consistent with our samples being heavily electron-doped, regardless of thickness. This result suggests that our electron-doping is more likely to be intrinsic to the layered material and not due to charge transfer from the substrate.

Our μ-ARPES measurements of 1-3ML and bulk WSe_2 along the high symmetry directions $\overline{M}$-$\overline{\Gamma}$-$\overline{K}$, given in Fig. 4, clearly show a transition in the occupied electronic structure with change in layer thickness. Superimposed on the measured data are the corresponding DFT-LDA band calculations, computed using ABINIT without spin-orbit interaction.[30][31] In the spectra, the distinctive features include the VBM at $\overline{\Gamma}$, derived from the W d_{z^2} and Se p_z orbitals, the VBM at $\overline{K}$, derived from the W $d_{x^2-y^2}/d_{xy}$ and Se p_x/p_y orbitals, and the valley between $\overline{\Gamma}$ and $\overline{K}$, derived from a crossover to the W $d_{x^2-y^2}/d_{xy}$

orbitals from the W d_{z^2} and Se p_z orbitals,[11][32][33] as shown and labeled in Fig. 4(a). Bands of higher binding energies and along other high-symmetry directions have been previously calculated and discussed in the literature.[11][23][24][32][33][34] These features are further displayed in the corresponding energy distribution curves (EDCs) [see Fig. 4(b)] and momentum distribution curves (MDCs) [see Fig. 4(c)]. Note that several of the WSe_2 bands are not detected in our ARPES measurements due to matrix-element selection rules as well as the above-mentioned difference in the photoionization cross-section between W- and Se-derived states. In our experiments, the incident photon flux was directed normal to the sample surface so that its polarization is in the plane of the WSe_2 crystal, thus suppressing excitation of states with out-of-plane character. This result explains why the W- and Se-derived states with a z or out-of-plane component, i.e., d_{z^2} or p_z orbital, in the uppermost valence band (UVB) near $\bar{\Gamma}$ have a consistently relatively weaker, but non-zero, intensity for 1-3ML and bulk WSe_2.

An important feature of our measurements is the change in the energy of the upper-most valence band (UVB) at $\bar{\Gamma}$ and $\bar{K}$ for 1ML WSe_2 compared to that of few-layer WSe_2. Our μ-ARPES spectra show that the valence band maximum is at $\bar{K}$ for 1ML WSe_2 and shifts to $\bar{\Gamma}$ for multilayer WSe_2. Previous reports[35][36][37][38][39] using traditional ARPES and inverse photoemission instruments have confirmed that the location of the VBM in bulk WSe_2 to be at $\bar{\Gamma}$; note that for bulk WSe_2, ARPES measurements over a large enough photon energy range are required in order to take into account the k_z dependence of the observed states. To fully quantify the VBM transition as a function of thickness, we used curvature analysis,[40] or the second-derivative method, to help delineate the electronic band structure, as shown in Fig. 5. Figures 5a-d give the bands for the 1-3ML and bulk WSe_2 samples, derived from the data in Fig.4 using this method, and with the zero energy referenced to the VBM. The UVB of exfoliated WSe_2 closely matches the corresponding calculated bands (white curves), except for the monolayer case where the measured energy difference between $\bar{\Gamma}$ and $\bar{K}$ is less than that predicted by theory, and where the dispersion at $\bar{\Gamma}$ is greater than that in the calculated bands. The experimentally measured and theoretically predicted[11] energy differences between $\bar{\Gamma}$ and $\bar{K}$ for monolayer and multilayer WSe_2 are plotted in Fig. 5e. The measured energy differences are: 0.21eV, -0.14eV, and -0.25eVfor 1-3ML; the value for bulk WSe_2 has been reported previously to be -0.3eV.[36][38] The error bars denote the standard deviation of the fittings from all six high symmetry equivalent directions, and they are well under the detector error of ±0.10eV. Thus, these results provide direct experimental evidence for a thickness-dependent shift in the relative energy of the VBM at $\bar{\Gamma}$ and at $\bar{K}$ and, hence, strong support for a shift from an indirect to a direct bandgap in going from 2 to 1 ML WSe_2.

An analysis of the curvature of the bands from the μ-ARPES measurements also allows us to deduce the effective mass of monolayer and bilayer WSe_2. For monolayer WSe_2, we determined an experimentally derived hole effective mass of $1.4\pm0.6m_0$ [41] (where m_0 is the electron mass) at $\bar{K}$, which is ~3x larger than theoretical predictions, and a hole effective mass of $3.5\pm1.8m_0$[41] at $\bar{\Gamma}$. The later quantity is approximately half as large as theoretical predictions ($7.1\pm0.2m_0$)[7][8][9][10][42]. For the case of bilayer WSe_2, however, we determined an experimentally derived hole effective mass of $0.4\pm0.1m_0$ at $\bar{K}$, which agrees well with theoretical predictions.[7][9] The origin of the discrepancy between experiment and DFT calculations for the case of a monolayer is uncertain at this time. Our

finite energy resolution does contribute to the measurement error. However, it is also apparent that there is an overall difference in band dispersion between our relatively simple theory calculation and experiment. This reasoning indicates that the above discrepancy is more complicated than simple instrumentation limits. Note that our DFT-derived effective-mass value of $0.44m_0$ for monolayer WSe_2 at $\overline{K}$ is in reasonable agreement with previous theoretical reports.[7][8][9][10] Also since $m_{eff} \propto \left|\frac{\partial^2 E}{\partial^2 k}\right|^{-1}$, slight measurement errors are accentuated by the flat-like dispersion curve in the vicinity of $\overline{\Gamma}$. "Renormalization" in bands of other 2D dichalcogenides have also been reported,[43][44] though the reason for this remains in question. Other possible explanations beyond that of an intrinsic nature of WSe_2 include effects of substrate interaction, such as strain, dielectric screening, etc.

In comparison to monolayer MoS_2, monolayer WSe_2 is expected to have an even larger spin-orbit splitting in the vicinity of $\overline{K}$, with a theoretically predicted value of ~0.46eV v.s. ~0.16eV of MoS_2.[11][45] The expected splitting of the valence band along the $\overline{\Gamma}$ - $\overline{K}$ direction of monolayer WSe_2 is due to the strong spin-orbit coupling originating from the high mass of the constituent elements and the lack of inversion symmetry.[11][45][46][47] The theoretically predicted value (~0.46eV) is larger than our experiment energy resolution and thus, should have been resolved directly in our measurements. However, despite the presence of an increasing linewidth of the UVB in the direction of $\overline{\Gamma}$-$\overline{K}$, which may be attributed to spin-orbit-splitting of the bands, we do not see two clear peaks in the vicinity of $\overline{K}$. We conjecture sample roughness, induced in the transfer process, is broadening the linewidth[48] of the spin-orbit split bands, leading to a broad unresolved band in our ARPES measurements. We have shown in previous works[22][44], using an analysis of LEED spot widths, that the transfer process introduces corrugation in monolayer MoS_2. Thus, resolving the spin-orbit-splitting in monolayer dichalcogenides is demanding in terms of a flat transfer procedure.

In conclusion, we have probed the surface structure and occupied electronic bands of 1 – 3 layer exfoliated WSe_2 crystals prepared by transfer to a native-oxide-terminated Si substrate. LEEM and μ-LEED provided real-space and reciprocal-space structural measurements of WSe_2, revealing clearly resolved thickness-dependent contrast and diffraction spot widths, respectively. Our μ-ARPES measurements have probed the occupied valence-band structure and confirmed the transition of the valence band maximum from $\overline{\Gamma}$ to $\overline{K}$ as the thickness is reduced from few-layer to 1ML WSe_2; this observation provides support for an indirect-to-direct bandgap transition. For monolayer WSe_2, we have found a lower bound of 1.8eV for the bandgap and measured a hole effective mass of 1.4 m_0 at $\overline{K}$ and 3.5 m_0 at $\overline{\Gamma}$. We expect that these results will provide insight to the understanding of the optical and electronic properties of monolayer and multilayer WSe_2 that is important for novel devices made from this transition-metal-dichalcogenide material.

ACKNOWLEDGEMENT

The beamline measurements and analyses and the sample mounting were supported by the Department of Energy, Office of Basic Energy Sciences, Division of Materials Sciences and Engineering under Award Contract No. DE-FG 02-04-ER-46157 and were carried out in part at the Center for Functional Nanomaterials and National Synchrotron Light Source, Brookhaven National Laboratory, which is supported by the U.S. Department of Energy, Office of Basic Energy Sciences, under Contract No. DE-AC02-98CH10886. The sample preparation and optical characterization (by D. Z., J. T. L., and I. P. H.) was supported as part of the Center for Re-Defining Photovoltaic Efficiency through Molecular Scale Control, an Energy Frontier Research Center funded by the U.S. Department of Energy (DOE), Office of Science, Office of Basic Energy Sciences under Award No. DE-SC0001085. The EFRC work is also supported by a matching grant from the Empire State Development's Division of Science, Technology and Innovation (NYSTAR) as well as by the New York State Energy Research Development Authority (NYSERDA).

REFERENCES

[1] Mak, K. F. *et al*. Atomically thin MoS_2: A new direct-gap semiconductor. *Phys. Rev. Lett.* **105**, 136805 (2010).

[2] Splendiani, A. *et al*. Emerging photoluminescence in monolayer MoS_2. *Nano Lett.* **10**, 1271–1275 (2010).

[3] Braga, D. *et al.* Quantitative determination of the band gap of WS_2 with ambipolar ionic liquid-gated transistors. *Nano Lett.* **12**, 5218–5223 (2012).

[4] Fang, H. *et al.* High-performance single layered WSe_2 p-FETs with chemically doped contacts. *Nano Lett.* **12**, 3788–3792 (2012).

[5] Yousefi, G. H. Optical properties of mixed transition metal dichalcogenide crystals. *Mater. Lett.* **9**, 38–40, (1989).

[6] Podzorov, V. *et al*. High-mobility field-effect transistors based on transition metal dichalcogenides. *Appl. Phys. Lett.* **84**, 3301– 3303 (2004).

[7] Kumar, A., Ahluwalia, P. K. Electronic structure of transition metal dichalcogenides monolayers 1H-MX2 (M = Mo, W; X = S, Se, Te) from ab-initio theory: new direct band gap semiconductors. *Eur. Phys. J. B* **85**:186 (2012)

[8] Ramasubramaniam, A. Large excitonic effects in monolayers of molybdenum and tungsten dichalcogenides. *Phys. Rev. B* **86**, 115409 (2012).

[9] Yun, W. S. *et al*. Thickness and strain effects on electronic structures of transition metal dichalcogenides: 2H-MX2 semiconductors (M = Mo, W; X = S, Se, Te). *Phys. Rev. B* **85**, 033305 (2012)

[10] Shi, H. *et al*. Quasiparticle band structures and optical properties of strained monolayer MoS_2 and WS_2. *Phy. Rev. B* **87**, 155304 (2013).

[11] Zhu, Z. Y. *et al*. Giant spin-orbit-induced spin splitting in two-dimensional transition-metal dichalcogenide semiconductors. *Phys. Rev. B* **84**, 153402 (2011).

[12] Liu, W. *et al.* Role of metal contacts in designing high-performance monolayer n-Type WSe_2 field effect transistors. *Nano Lett.* **13** (5), 1983–1990 (2013).

[13] Jones, A. M. *et al*. Optical generation of excitonic valley coherence in monolayer WSe_2.*Nature Nanotech.* **8**, 634–638 (2013).

[14] Mak, K. F. *et al*. Tightly bound trions in monolayer MoS_2. *Nature Mater.* **12**, 207–211 (2013).

[15] Ross, J. S. *et al*. Electrical control of neutral and charged excitons in a monolayer semiconductor. *Nature Commun.* **4**, 1474 (2013).

[16] Sadowski, J. T. Pentacene growth on 3-aminopropyltrimethoxysilane modified silicon dioxide. *Optical Materials* **34**, 1635-1638 (2012).

[17] Sutter, P. *et al*. Electronic structure of few-layer epitaxial graphene on Ru(0001). *Nano Lett.* **9**, 2654 (2009).

[18] Zeng, H. L. *et al*. Optical signature of symmetry variations and spin-valley coupling in atomically thin tungsten dichalcogenides. *Sci. Rep.* **3**, 1608 (2013).

[19] Zhao, W. J. *et al*. Evolution of electronic structure in atomically thin sheets of WS_2 and WSe_2 *ACS Nano* **7** (1) 791–797 (2013).

[20] Seah, M. P. and Dench, W. A., Quantitative electron spectroscopy of surfaces: A standard data base for electron inelastic mean free paths in solids. *Surf. Interface Anal.*, **1**: 2–11 (1979).

[21] Kalikhman, V. L.; Umanskii, Y. S. Transition-metal chalcogenides with layer structure and features of the filling of their Brillouin zones. *Sov. Phys.-Usp.* **15**, 728-740 (1973).

[22] Yeh, P.-C. *et al.* Probing substrate-dependent long-range surface structure of single- and multi-layered MoS_2 by low-energy electron microscopy and microprobe diffraction. *Phys. Rev. B* **89**, 155408 (2014).

[23] Mattheiss, L. Band Structures of transition-metal-dichalcogenide layer compounds. *Phys. Rev. B* **64**, 235305 (2001).

[24] Coehoorn, R. *et al*. Electronic structure of $MoSe_2$, MoS_2, and WSe_2. I. Band-structure calculations and photoelectron spectroscopy. *Phys. Rev. B* **35**, 6195 (1987).

[25] Yeh, J. J. and Lindau, I. Atomic subshell photoionization cross sections and asymmetry parameters: 1 <= Z <= 103. *At. Data Nucl.* Data tables **32**, 1 (1985).

[26] Deshpande, M. P. *et al.* Optical band gap in tungsten diselenide single crystals intercalated by indium. *Mater. Lett.* **43(1-2)**, 66–72 (2000).

[27] Wilson, J. A. and Yoffe, A. D. The transition metal dichalcogenides discussion and interpretation of the observed optical, electrical and structural properties. *Adv. Phys.* **18**(73), 193-335 (1969).

[28] Spah, R. *et al*. Pn Junctions in tungsten diselenide. *Appl. Phys. Lett.* **43**, 79 (1983).

[29] Upadhyayula, L.C. *et al*. Semiconducting properties of single crystals of n- and p-type tungsten diselenide (WSe_2). *J. Appl. Phys.* **39**, 353-358 (1968).

[30] Gonze, X. *et al.* A brief introduction to the ABINIT software package. *Z. Kristallogr.* **220**, 558 (2005).

[31] Gonze, X. *et al*. ABINIT: First-principles approach to material and nanosystem properties. *Comput. Phys. Commun.* **180**, 2582 (2009).

[32] Liu, G.-B. *et al.* Three-band tight-binding model for monolayers of group-VIB transition metal dichalcogenides. *Phys. Rev. B* **88**, 085433 (2013).

[33] Cappelluti, E. *et al.* Tight-binding model and direct-gap/indirect-gap transition in single-layer and multilayer MoS_2. *Phys. Rev. B* **88**, 075409 (2013).

[34] Klein, A. *et al*. Electronic band structure of single-crystal and single-layer WS_2: Influence of interlayer van der Waals interactions. *Phys. Rev. B* **64**, 205416 (2001).

[35] Straub, Th. *et al*. Valence-band maximum in the layered semiconductor WSe_2: Application of constant-energy contour mapping by photoemission. *Phys. Rev. B* **53**, R16152(R) (1996).

[36] Finteis Th. *et al*. Occupied and unoccupied electronic band structure of WSe_2. *Phys. Rev. B* **55**, 10400 (1997).

[37] Finteis Th. *et al*. Erratum: Occupied and unoccupied electronic band structure of WSe_2 [Phys. Rev. B 55, 10400 (1997)]. *Phys. Rev. B* **59**, 2461 (1999).

[38] Traving M. *et al.* Electronic structure of WSe_2: A combined photoemission and inverse photoemission study. *Phys. Rev. B* **55**, 10392 (1997).

[39] Yu, S.-W. *et al.* Spin resolved photoemission spectroscopy on WSe_2. *J. Electron. Spectrosc. Relat. Phenom.* **101–103** (1999).

[40] Zhang P. *et al*. A precise method for visualizing dispersive features in image plots. *Rev. Sci. Instrum*. **82** 043712 (2011).

[41] The estimated error here is a combination of the standard error in parabolic fitting and the standard deviation of the effective mass along different high symmetry directions.

[42] Based on our DFT-LDA calculation.

[43] Zhang, Yi, *et al.* Direct observation of the transition from indirect to direct bandgap in atomically thin epitaxial $MoSe_2$. *Nature Nanotech.* **9**, 111–115 (2014).

[44] Jin, W. *et al*. Direct Measurement of the thickness-dependent electronic band structure of MoS_2 using angle-resolved photoemission spectroscopy. *Phys. Rev. Lett.* **111** (10) 106801 (2013).

[45] Kośmider, K. *et al*. Large spin splitting in the conduction band of transition metal dichalcogenide monolayers. *Phys. Rev. B* **88**, 245436 (2013).

[46] Xiao, D. *et al.* Berry phase effects on electronic properties. *Rev. Mod. Phys.* **82**, 1959 (2010).

[47] Xiao, D. *et al*. Coupled Spin and Valley Physics in Monolayers of MoS_2 and Other Group-VI Dichalcogenides. *Phys. Rev. Lett.* **108**, 196802 (2012).

[48] Knox, K. R. *et al*. Making angle-resolved photoemission measurements on corrugated monolayer crystals: Suspended exfoliated single-crystal graphene. *Phys. Rev. B* **84**, 115401 (2011).

[49] Flege, J. I. *et al*. A new soft X-ray photoemission microscopy beamline at the National Synchrotron Light Source. *Nucl. Instrum. And Meth. B* **261**, 855 (2007).

[50] See the Supplemental Material section of the paper: http://link.aps.org/supplemental/10.1103/PhysRevLett.111.106801 for more details about sample preparation, ARPES configuration, and matrix-element analysis.

[51] Sutter, P. and Sutter, E. Microscopy of graphene growth, processing, and properties. *Adv. Funct. Mater.* **23**, 2617 (2013).

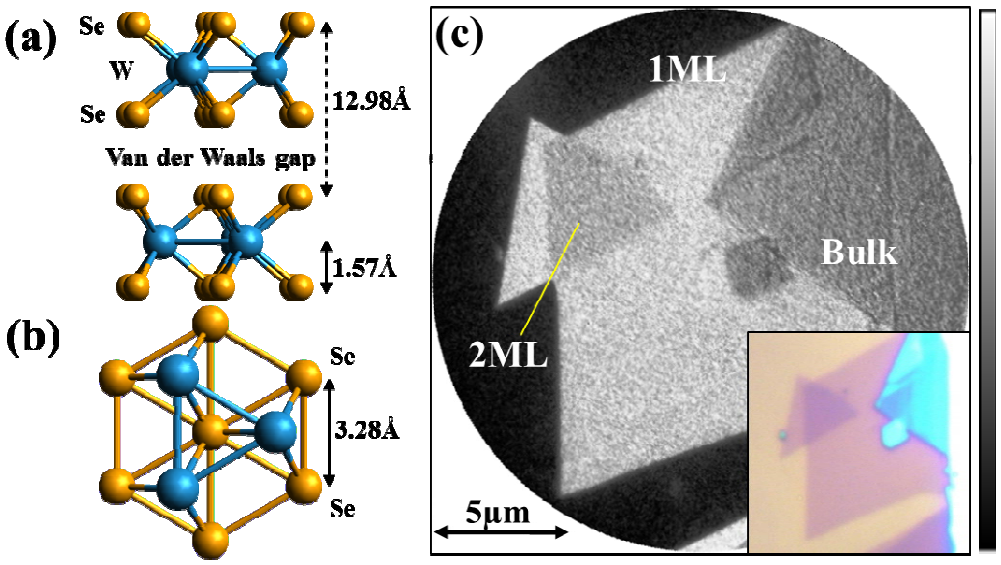

Figure 1 (a) Side view and (b) top view of the trigonal prismatic coordination of the atoms in 2H-WSe_2. (c) LEEM image of 1ML WSe_2 after transfer (detector artifacts and background signal have been removed.) The inset is the corresponding optical microscope image of the same sample. LEEM images were taken at an electron energy of 1.8eV.

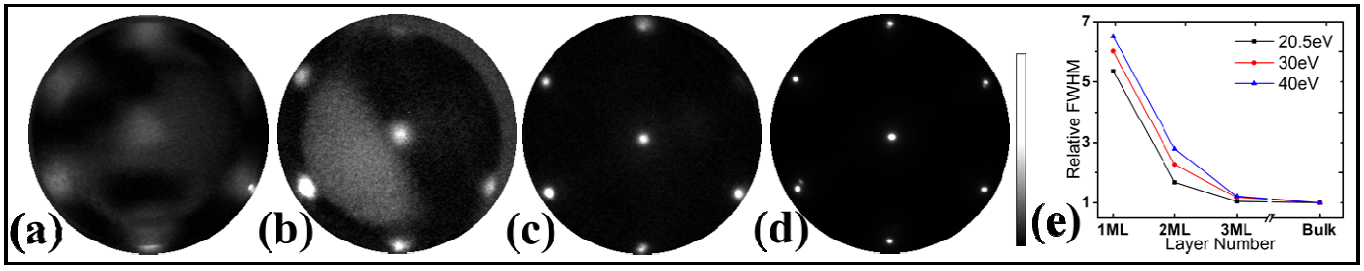

Figure 2: (a)-(d) Micro-LEED patterns at 48eV electron energy on exfoliated WSe_2 1 ML (a), 2 ML (b), 3 ML (c), and bulk (d) after transfer to Si. The halo around 1ML (00) spot came from edge deflection of electrons due to a limited sample size. (e) Measured FWHM of the (00) LEED spot for 1-3ML WSe_2 flakes relative to that of bulk, measured at 20.5, 30, and 40eV electron energy. The FWHM decreases with increasing number of layers, since electrons elastically backscattered from the Si substrate are progressively decreased.

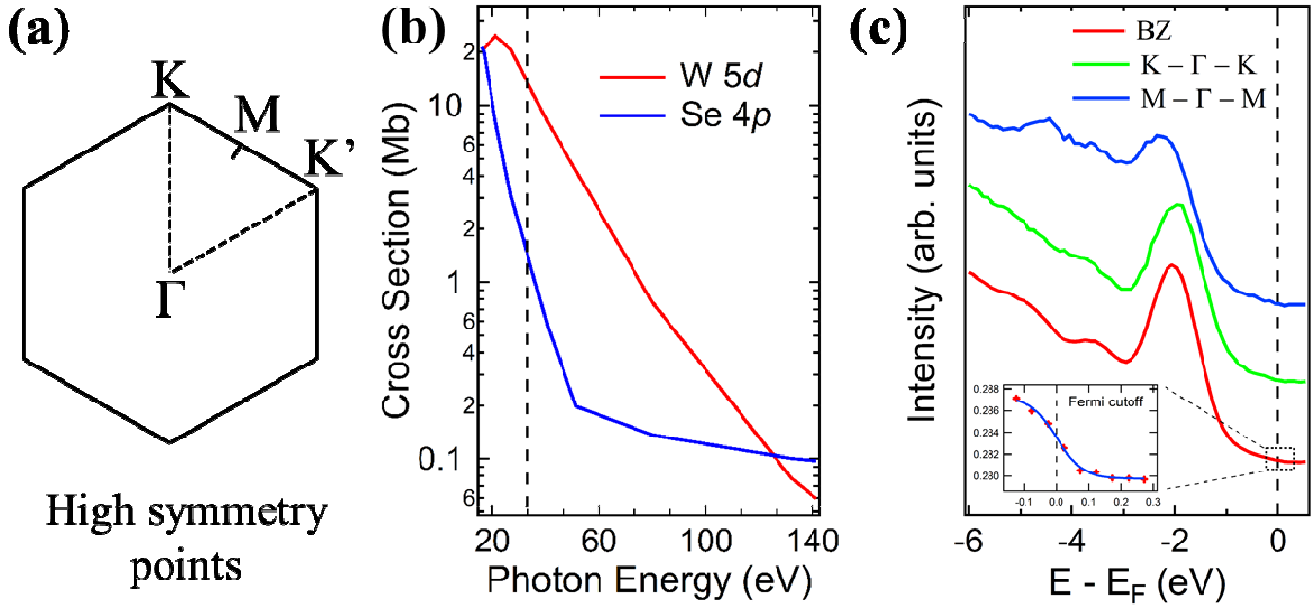

Figure 3: (a) Brillouin zone and high-symmetry points of WSe_2. (b) Atomic photoionization cross-section for W 5d and Se 4p subshells as a function of ARPES photon energy.[25] At 33eV, the cross-section between W 5d and Se 4p has an order-of-magnitude difference. Therefore, the dominant features in our ARPES measurement are the contribution of W 5d subshell. Note that the Cooper minimum of the Se orbital is ~50eV. (c) Angle-integrated photoemission spectra of monolayer WSe_2 extracted from high symmetry directions K-Γ-K and M-Γ-M, and over the full BZ, referenced with respect to the Fermi level.

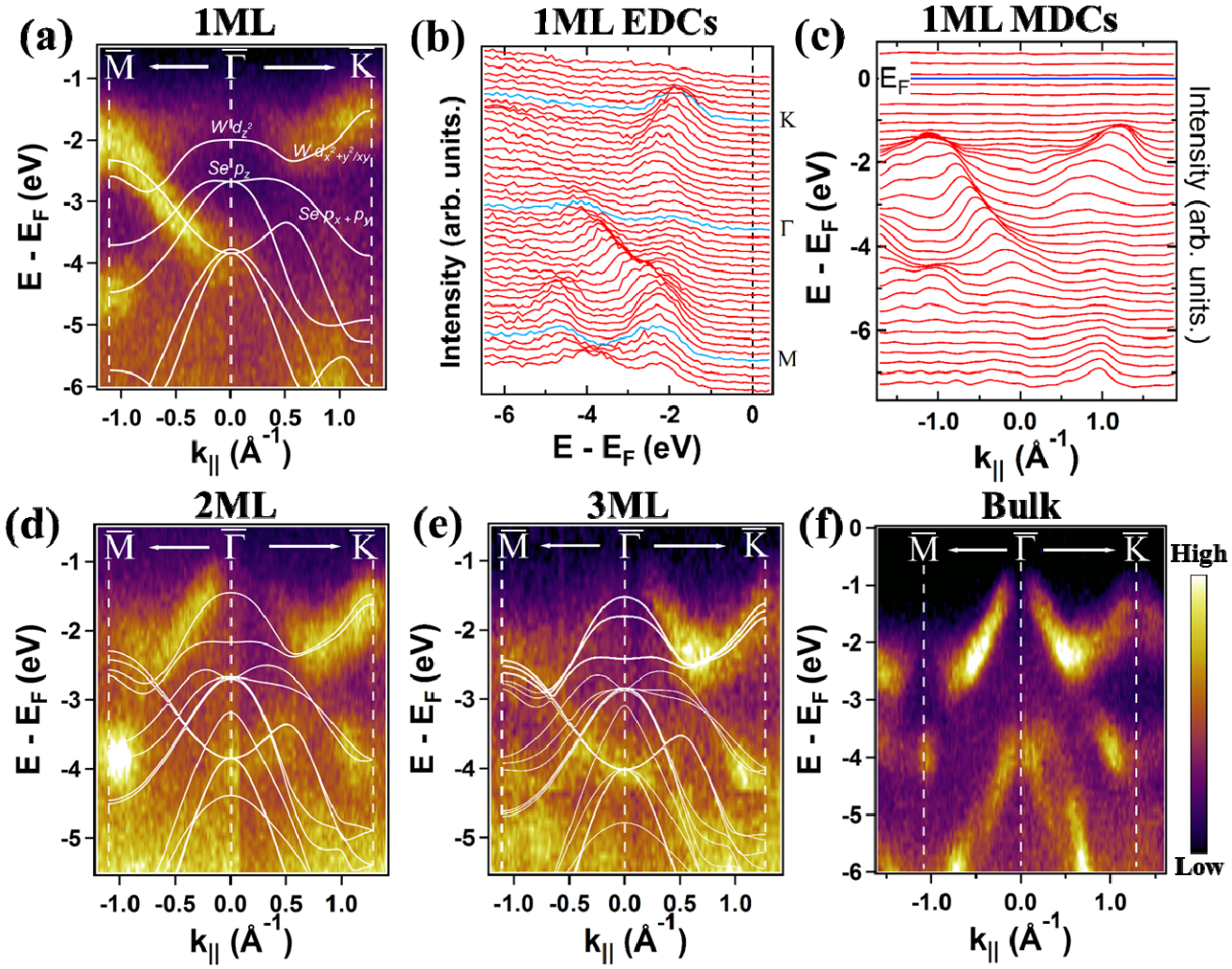

Figure 4: μ-ARPES band mapping of exfoliated WSe_2 for (a) 1ML (d) 2ML (c) 3ML and (f) bulk along the high-symmetry path M-Γ-K in the Brillouin zone. E=0 denotes the Fermi level. The overlaid white lines are our DFT-calculated band structures. The calculations do not include the effect of spin-orbit coupling. (b), (c) Corresponding EDCs and MDCs of 1ML WSe_2, respectively.

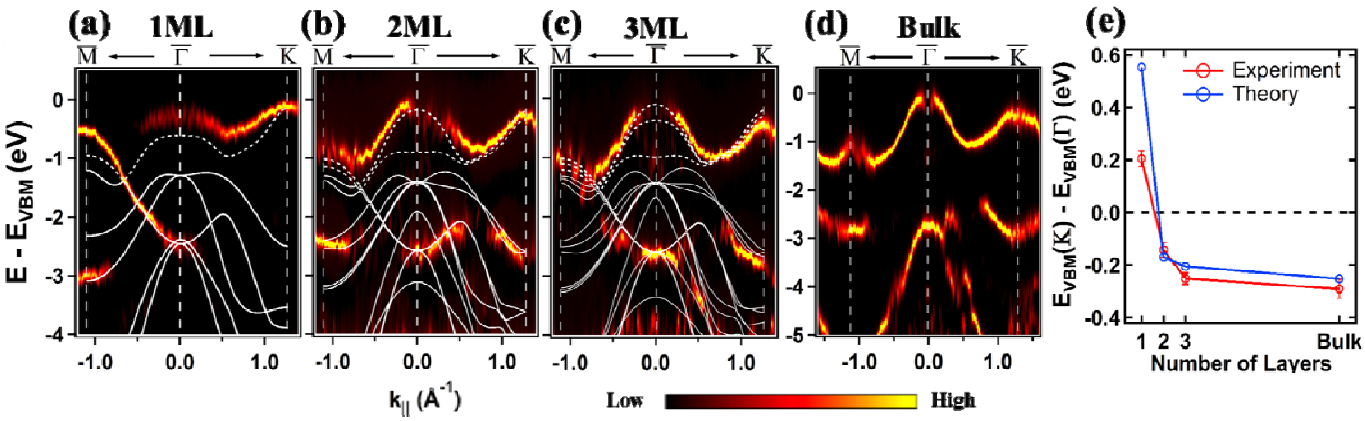

Figure 5 (a)-(d) Second derivatives of the low-energy valence bands along high symmetry points of exfoliated 1-3ML and bulk WSe_2, respectively, generated from the μ-ARPES band maps of Fig. 4. The white lines are the corresponding DFT-calculated bands as in Fig. 4. The dashed-white lines refer to the top valence bands, which illustrate the layer-number dependence of the electronic structure near the VBM. Here the energy scale is set to zero at the VBM. (e) Layer-number-dependent VBM transition in terms of energy difference between K and Γ points. The error bars denote the standard deviation of the fittings from all six high symmetry equivalent directions, and they are well under the detector error of ±0.10eV. The theoretical and experimental results are plotted for comparison.